

Tensor-network representation of excitations in Josephson junction arrays

Emilio Rui,^{1,2,*} Joachim Cohen,^{1,§} and Alexandru Petrescu^{2,§}

¹Alice and Bob, 53 Bd du Général Martial Valin, 75015 Paris, France

²Laboratoire de Physique de l'École Normale Supérieure,
École Normale Supérieure, Centre Automatique et Systèmes,
Mines Paris, Université PSL, CNRS, Inria, Paris, France

(Dated: October 13, 2025)

We present a nonperturbative tensor-network approach to the excitation spectra of superconducting circuits based on Josephson junction arrays. These arrays provide the large lumped inductances required for qubit designs, yet their intrinsically many-body nature is typically reduced to effective single-mode descriptions. Perturbative treatments attempt to include the collective array modes neglected in these approximations, but a fully nonperturbative analysis is challenging due to the many-body structure and the collective character of these modes. We overcome this difficulty using the DMRG-X algorithm, which extends tensor-network methods to excited states. Our key advance is a construction of trial states from the linearized mode structure, enabling direct computation of excitations, even in degenerate manifolds, which was previously inaccessible. Our results reveal significant deviations from, and allow us to improve upon, previous perturbative treatments in the regime of low array junction impedance.

Introduction. Large, lumped linear inductors are critical components in the design of modern superconducting quantum circuits for quantum information processing. Inductive shunts of this kind are central to various architectures, including lumped-element LC resonators [1], the fluxonium qubit [2], protected qubits, such as the $0 - \pi$ qubit [3], or based on Cooper-pair pairing [4, 5], and the asymmetrically threaded SQUID (ATS) [6, 7]. These shunts are typically realized using arrays of Josephson junctions – so-called superinductors – that achieve impedances exceeding the resistance quantum [1, 2, 8, 9]. Josephson junction arrays are as well central to the design of near-quantum-limited amplifiers [10–12].

In standard circuit quantization approaches, superinductors are modeled as a single lumped linear inductor, with the total phase drop across the array treated as a single dynamical variable (Fig. 1). In reality, however, each junction in the array has its own phase degree of freedom, giving rise to a set of collective chain or array modes [13–16]. In typical implementations, the frequencies of these additional modes lie well above those of the fundamental modes relevant to the effective theory. Nonetheless, they could couple nontrivially to the low-energy sector, particularly in the presence of circuit imperfections [13], nonlinearities [14], or external parametric drives [17]. Such couplings could lead to spurious effects [14, 17], underscoring the need for accurate modeling.

In this Letter, we nonperturbatively study the excitation spectrum related to the internal-mode structure of Josephson-junction arrays, using tensor-network methods [18–21]. Previous work has shown that tensor networks can efficiently represent the low-lying spectra of fluxonium qubits [22, 23], while accurately accounting for the many-body structure of the Josephson junction

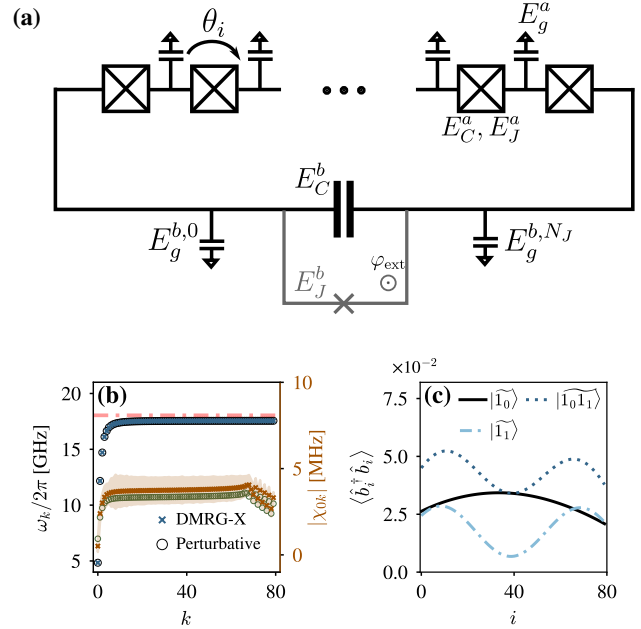


FIG. 1. (a) Lumped LC resonator obtained through a capacitively shunted superinductance. The fluxonium qubit circuit is obtained by closing the loop with a small shunt “black sheep” junction (in grey). (b) DMRG-X-computed frequencies of the chain modes (blue crosses) compared to perturbation theory (black circles), and cross-Kerr nonlinearities χ_{0k} between the k^{th} mode and the fundamental mode (orange crosses) compared to perturbation theory (green circles). The shaded area indicates the uncertainty of the DMRG-X results, while the pink dot-dashed line marks the plasma frequency of the junctions in the array. (c) Chain-site occupation $\langle \hat{b}_i^\dagger \hat{b}_i \rangle$ as a function of site index i for the single-excitation states corresponding to the fundamental mode $|\widetilde{1}_0\rangle$ (solid line) and the first mode $|\widetilde{1}_1\rangle$ (dot-dashed line), and for the two-excitation state $|\widetilde{1}_0\widetilde{1}_1\rangle$ (dotted line).

Set	N_J	E_J^a	E_C^a	E_J^b	E_C^b	E_g^a	$E_g^{b,0}$	E_g^{b,N_J}
1[1, 14]	80	84.3	0.483	0	6.07	170	3.45	5.91
2 [14]	43	26.0	1.24	8.93	3.60	194	4.80	4.80
3[22]	40	–	–	8.9	2.58	194	194	194

TABLE I. Device parameters for the three parameter sets. All energies are in GHz. The first parameter set describes the LC resonator studied in Fig. 1, the second in Fig. 2. The third parameter set describes Fig. 3. The missing terms are function of the array’s junction impedance z and their plasma frequency $\omega_p = 12.5\text{GHz}$

array. Inspired by this, we focus here on the high frequency internal array modes, which, due to their high frequency and near-degeneracies around the characteristic plasma frequency, are numerically challenging. To address this challenge, we employ the DMRG-X algorithm [24], a variant of the density-matrix renormalization group (DMRG)[18, 19] designed to target individual excited states [24]. We thus exploit a recently pointed out correspondence between non-chaotic states in superconducting circuits and many-body localized systems [25, 26].

DMRG-X enables the nonperturbative computation of excited states, provided a good initial trial state. It has previously been used as an effective diagonalization tool on top of black-box quantization approaches [27–30]. In this Letter, we extend this idea by developing a strategy to construct trial states from the normal modes of the linearized system, but perform no approximation at the level of the Hamiltonian. While we focused here on Josephson junction arrays – particularly challenging for previous methods due to their degenerate spectrum – this approach could be used for the nonperturbative study of systems usually treated by BBQ methods [31, 32], without however expanding the Josephson nonlinearity [25, 26, 29, 30, 33].

We apply this framework to two experimentally relevant systems (Fig. 1). First, we consider a lumped-element LC resonator composed of a Josephson-junction array superinductance capacitively shunted [1], demonstrating that DMRG-X enables efficient and accurate resolution of the full spectrum of single-excitation chain modes. Second, we study the fluxonium qubit, focusing on the cross-Kerr nonlinearity between its fundamental mode and the most strongly coupled chain mode [14]. Our simulations reveal substantial quantitative deviations from previous perturbative predictions [14, 17], highlighting the capability of the method to both validate and refine such approximations. Building on this, we propose improvements to perturbative treatments that significantly enhance their accuracy. We eventually show that the method effectively captures charge-offset effects in the array [22, 34, 35] by analyzing a fluxonium device whose superinductor is formed from more strongly

nonlinear, high-impedance junctions.

Model. The system we study, depicted schematically in Fig. 1, is a superinductor of N_J junctions, shunted either by a capacitor, realizing a lumped-element LC resonator [1], or by a small Josephson junction with a capacitance, realizing the fluxonium qubit [2]. The Hamiltonian describing this circuit [22] is

$$\hat{H} = \sum_{i=1}^{N_J} \hat{H}_{0,i} + \sum_{i,j=1}^{N_J} \hbar g_{ij} (\hat{n}_i - n_{g,i}) (\hat{n}_j - n_{g,j}) + U \left(\sum_{i=1}^{N_J} \hat{\theta}_i \right), \quad (1)$$

where $\hat{H}_{0,i}$ is a transmon-like Hamiltonian [36] describing the i^{th} junction in the array,

$$\hat{H}_{0,i} = 4E_{C,i}(\hat{n}_i - n_{g,i})^2 - E_{J,i} \cos \hat{\theta}_i, \quad (2)$$

with $E_{J,i}$ the Josephson energy of the junction, $E_{C,i}$ its charging energy. We explicitly include possible offset charges $n_{g,i}$ at each junction [22]. The second term in Eq. (1) accounts for long-range capacitive couplings set by the array layout and the shunt element [37]. The final contribution is the nonlinear potential of the black-sheep junction,

$$U \left(\sum_i \hat{\theta}_i \right) = -E_J^b \cos \left(\sum_i \hat{\theta}_i + \varphi_{\text{ext}} \right), \quad (3)$$

with $\varphi_{\text{ext}} = 2\pi\Phi_{\text{ext}}/\Phi_0$ the dimensionless external flux and Φ_0 the flux quantum. The lumped-element LC resonator is recovered in the limit $E_J^b = 0$.

We represent the Hamiltonian Eq. (1) nonperturbatively as a matrix product operator (MPO) by expressing it in the eigenbasis of the local Hamiltonians Eq. (2),

$$\hat{H}_{0,i} = \sum_{k=0}^{\infty} E_k^{(i)} |\psi_k^{(i)}\rangle \langle \psi_k^{(i)}|. \quad (4)$$

This representation, developed in Ref. [22] [37], enables an efficient description of Eq. (1) while retaining the $n_{g,i}$ -dependent charge effects [36]. However, in this basis the system’s eigenstates are not well captured by tensor-product states $\bigotimes_{i=1}^{N_J} |\psi_{k_i}^{(i)}\rangle$. In superinductors, the junctions are designed to be uniform, and this symmetry [13–15] gives rise to collective excitations of the array. This poses a challenge for DMRG-X [24], which relies on tensor-product states of the local orbitals Eq. (4) – so-called l -bit strings [29, 30] – as initial guesses.

To address this, we leverage the normal modes of the linearized system [31, 32] as efficient starting points for constructing excited states with DMRG-X. Inspired by natural-orbital approaches [38–40], we generalize the notion of a target state by promoting the l -bit string to

a string of nonnegative occupation numbers l_i associated with the normal modes defined below,

$$|l_k\rangle_{\text{trial}} = \prod_{k=1}^{N_J} (\hat{A}_k^\dagger)^{l_k} |\Psi_0\rangle, \quad (5)$$

where $|\Psi_0\rangle$ is a reference state, typically the many-body ground state, and \hat{A}_i^\dagger denotes a finite-dimensional creation operator of the i^{th} normal mode. To construct these operators, we start from ladder operators in the local eigenbasis,

$$\hat{b}_i = \sum_{k=1}^D \sqrt{k} |\psi_{k-1}^{(i)}\rangle \langle \psi_k^{(i)}|. \quad (6)$$

which reduce to *bona fide* bosonic operators in the limit $D \rightarrow \infty$. The normal-mode operators \hat{A}_i are then obtained via the symplectic transformation S that diagonalizes the linearized Hamiltonian [37, 41–44],

$$\hat{\mathbf{A}} = S\hat{\mathbf{b}}, \quad (7)$$

with $\hat{\mathbf{A}} = (\hat{A}_0, \hat{A}_0^\dagger, \hat{A}_1, \dots)^\top$ and $\hat{\mathbf{b}} = (\hat{b}_0, \hat{b}_0^\dagger, \hat{b}_1, \dots)^\top$. While the coefficients in S follow from a linear approximation, this affects only the construction of the trial state $|l_k\rangle$ in Eq. (5). The variational refinement in DMRG-X is then performed with the full MPO representation of the nonlinear Hamiltonian Eq. (1), yielding the converged excited state $|\tilde{l}_k\rangle$.

Equation (1) encompasses a broad class of superconducting circuit Hamiltonians, beyond the specific superinductor configuration considered here [25, 33]. The strategy we propose – based on determining a set of natural excitations in a well controlled limit of the problem, and building trial states by constructing these excitations on top of a correlated reference state – also applies to other architectures where a tensor-product trial state based on local orbitals may be inadequate. This could include fluxon lattices [45], transmon [25, 29, 30], and fluxonium arrays [29].

Lumped LC resonator. We benchmark our method on a lumped-element LC resonator implemented as a capacitively shunted array of 80 Josephson junctions [1]. The circuit is shown in black in Fig. 1a), with circuit parameters given in Table I, first row. This system is weakly anharmonic, and thus serves as an ideal testbed to validate our approach. We first probe the single-excitation manifold; to do so, we use as a reference state $|\psi_{gs}\rangle$ the ground state of the system using the standard DMRG technique [18, 19]. Note that $\hat{A}_k |\psi_{gs}\rangle \approx 0$, with exact equality in the harmonic limit. We consider trial states based upon Eq. (5) corresponding to single excitations in the k^{th} mode, that is $l_k = 1$ while $l_{k'} = 0$ for all $k' \neq k$.

Figure 1b) compares the resulting excitation spectrum with predictions from perturbation theory based on black-box quantization [31, 32, 37, 46]. Our DMRG-X method converges to each of the N_J single-excitation

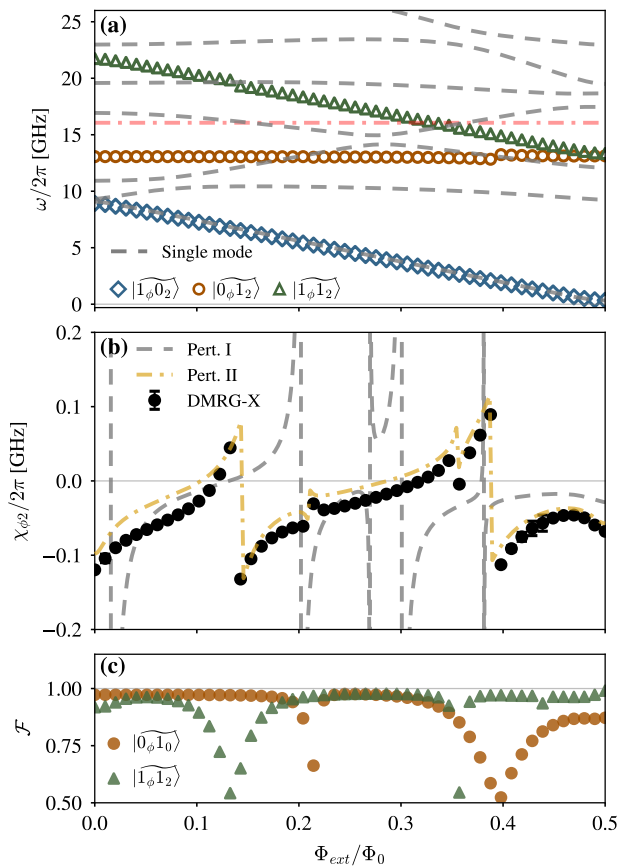


FIG. 2. DMRG-X applied to the Fluxonium qubit. (a) Fluxonium energy spectrum as a function of the external flux φ_{ext} threading the circuit. The dashed gray lines show the effective-theory prediction from Ref. [22], while the dot-dashed pink line marks the plasma frequency of the junctions in the array. Blue markers denote the fluxonium state $|\widehat{1}_\phi 0_2\rangle$ computed via DMRG, and orange and green markers indicate, respectively, the states $|\widehat{0}_\phi 1_2\rangle$ and $|\widehat{1}_\phi 1_2\rangle$ computed with DMRG-X. (b) Cross-Kerr interaction $\chi_{\phi 2}$ between the fluxonium qubit and the first even chain mode. Dots represent the nonperturbative DMRG-X results. The dashed gray line shows the perturbative prediction from Ref. [14], while the orange dot-dashed line includes corrections to the chain-mode frequency [37]. (c) Fidelity $\mathcal{F} = \langle \psi_{\text{trial}} | \psi \rangle$ between the DMRG-X-computed eigenstate $|\psi\rangle$ and the trial state $|\psi_{\text{trial}}\rangle$.

eigenstates and resolves their quasi-degenerate structure. The accuracy of each state, estimated from the energy variance, $\sigma = (\langle H^2 \rangle - \langle H \rangle^2)^{1/2}$, remains below 1 MHz. We achieve this small error bar by modifying the DMRG-X local optimization step [24] including shift-invert iterations [29, 47–50].

There is a slight renormalization of the mode frequencies compared to the linear normal modes, which becomes manifest in the slight discrepancy between the asymptotic, large k value of the normal mode frequencies and the plasma frequency of the junctions. This correction

is naturally captured by our nonperturbative approach, and is also accurately described by black box quantization based perturbation theory [31, 32, 37]. Note that this contribution, with exceptions [16], has typically been neglected in previous analyzes of chain modes [1, 14, 17].

Beyond the single-excitation sector, we access the two-excitation spectrum and compute cross-Kerr couplings between the fundamental mode and the other modes χ_{0j} as defined by the following Walsh-Hadamard transform [25]

$$\chi_{ij} = \frac{1}{2} \left[E(|\widetilde{1_1 1_j}\rangle) - E(|\widetilde{1_i 0_j}\rangle) - E(|\widetilde{0_1 1_j}\rangle) \right], \quad (8)$$

with the understanding that all other modes have $l_k = 0$, and all energies are measured relative to the ground state. These nonlinear couplings χ_{0j} , shown in Fig. 1, are frequently used in experiments to measure the frequencies of the chain modes [1, 16].

The computation of these quantities is typically prohibitive for standard DMRG methods, which must resolve the full spectrum up to the target excitation and therefore incur a large computational overhead [19, 23]. In addition, the relevant eigenstates are poorly represented in the tensor-product basis of local eigenstates $|\psi_k^{(i)}\rangle$ of the junction Hamiltonian $\hat{H}_{0,i}$ in Eq. (2), rendering a standard DMRG-X implementation unfeasible. To illustrate this, we evaluate the junction occupations $\langle \hat{b}_i^\dagger \hat{b}_i \rangle$ for some single-excitation states. As shown in Fig. 1c), the resulting profiles follow the standing-wave patterns of the array [1], emphasizing their collective nature.

Fluxonium qubit. We now extend our investigation to a regime of stronger nonlinearity by considering the fluxonium qubit [2, 14]. This circuit is described by the superinductor in Eq. (1) together with the potential energy Eq. (3) of a single small Josephson junction – the ‘black sheep’ – which introduces strong anharmonicity. Effective theories [14, 17] show that the nonlinearity of the black sheep predominantly affects the fundamental mode of the system, which becomes the ‘fluxonium mode’, denoted $\phi = \sum_{i=1}^{N_j} \theta_i$, while higher-frequency array modes are relatively weakly perturbed by Eq. (3). The residual coupling between the fundamental and the array modes, which can degrade the coherence time of the fluxonium qubit [14, 17], is well encapsulated by cross-Kerr interactions $\chi_{\phi i}$ of Eq. (8).

To compute $\chi_{\phi i}$, we extend the approach used for the LC resonator. Being strongly anharmonic, the excitations of the fluxonium mode are not well captured by the trial states Eq. (5). Exploiting the fact that the nonlinear fluxonium mode is the fundamental 0^{th} mode [13, 14], we first obtain the ground and first excited states of the full fluxonium Hamiltonian Eq. (1) using standard DMRG techniques [22, 51, 52], yielding two reference states $|\Psi_0\rangle = |\widetilde{0_\phi}\rangle$ and $|\widetilde{1_\phi}\rangle$, where all the other modes are in their vacuum. For example, to build the state $|\widetilde{1_\phi 1_i}\rangle$ with one excitation in both the fluxonium and the

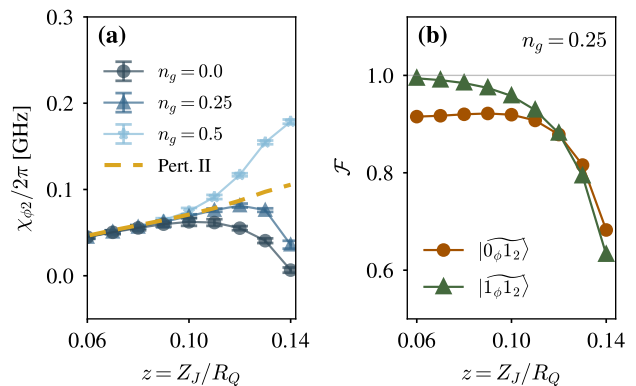


FIG. 3. Charge dispersion of the cross-Kerr $\chi_{\phi 2}$ in a fluxonium based on a 40-junction superinductance [22] while increasing the array junction impedance $z = Z/R_Q$ at half flux quantum $\Phi_{\text{ext}}/\Phi_0 = 0.5$. The circuit parameters are listed in Table I. (a) $\chi_{\phi 2}$ between the fluxonium qubit and the second chain mode for a uniform gate charge in the array (solid lines) against the perturbative approach in the dashed line. (b) Fidelity $\mathcal{F} = \langle \psi_{\text{trial}} | \tilde{\psi} \rangle$ of the DMRG-X computed eigenstates $|\tilde{\psi}\rangle$ and the trial states for $n_g = 0.25$.

i^{th} chain mode, we construct $|\psi_{\text{trial}}\rangle \equiv |1_\phi 1_i\rangle = \hat{A}_i^\dagger |\widetilde{1_\phi 0_i}\rangle$, where $|\widetilde{1_\phi 0_i}\rangle$ is the first excited state of the fluxonium system with no added excitation in mode i .

We focus on the interaction between the fluxonium mode and the lowest even-parity array mode ($k = 2$), which couples most strongly to the qubit [14]. Figure 2a) shows the circuit spectrum, for the parameters in Table I-2, as a function of the external flux φ_{ext} . The single qubit excitation $|\widetilde{1_\phi}\rangle$ (blue circles) is obtained with standard DMRG as explained above, while the DMRG-X results for $|\widetilde{0_\phi 1_i}\rangle$ and $|\widetilde{1_\phi 1_i}\rangle$ are shown in orange and green, respectively. The corresponding cross-Kerr interaction $\chi_{\phi 2}$ is plotted in Fig. 2b).

The DMRG-X results (dots) show significant deviations from previous perturbative predictions (Pert. I) [14], particularly near resonances and around the typical operating point $\Phi_{\text{ext}}/\Phi_0 = 0.5$. Notably, our method converges reliably even close to degeneracies, where the quality of the trial states is expected to deteriorate. This is confirmed by the fidelity $\mathcal{F} = \langle \psi_{\text{trial}} | \tilde{\psi} \rangle$ in Fig. 2c), which remains high across the flux range, aside from the expected drops at avoided crossings. The nonperturbative character of our approach thus makes it a powerful benchmark for perturbation theory. To this end, we refine previous treatments by incorporating the renormalization of chain-mode frequencies induced by array nonlinearities [Pert. II in Fig. 2b)], which substantially improves agreement [37].

Offset-charge dependence—The method proposed in this Letter retains the 2π -periodic form of the Josephson potential and thus the compactness of the phase variables θ_i [22]. While alternative approaches expand the

Josephson potentials in the Hamiltonian [53], we keep their full form [37]; the only approximations enter in the construction of trial states for DMRG-X. This allows us to capture offset-charge effects arising from the charges $n_{g,i}$ included in the Hamiltonian Eq. (1), which, through the Aharonov-Casher effect [54–56], determine the phase of coherent quantum phase slips (CQPS) in the array [2, 34, 36, 57–60].

The fluxonium qubit provides a sensitive probe of coherent quantum phase slips (CQPS) [2, 61], as the black-sheep junction acts as a weak link in the array and CQPS lead to broadening of the qubit transition frequency. The CQPS rate depends exponentially on the reduced junction admittance $1/z$, making the effect increasingly pronounced for higher-impedance junctions. This regime has been previously investigated using tensor-network methods [22]. Following the same strategy as in Fig. 2, we employ DMRG-X to study the offset-charge dependence of the cross-Kerr coupling $\chi_{\phi 2}$ between the fluxonium and the $k = 2$ chain mode in arrays with progressively larger impedance.

In Fig. 3, we examine the effect of a uniform offset charge $n_{g,i} = n_g$ on the z -dependence of the cross-Kerr coupling $\chi_{\phi 2}$ between the fluxonium qubit biased at the half-flux point and the second collective mode of a 40-junction array. As expected, CQPS become increasingly relevant at large z [2], inducing strong gate-charge sensitivity in the spectrum. In this high-impedance regime, the perturbative approach fails as it neglects the charge dispersion of the chain islands, with better agreement expected at $n_g = 0.25$ where destructive interference suppresses coherent quantum phase slips [36]. Nevertheless, our DMRG-X method converges across the entire range of impedance z explored. We observe that the fidelity to the trial states decreases in the deep nonlinear regime, reflecting the breakdown of the harmonic approximation underlying their construction. Importantly, however, the method continues to converge even for large impedances $z > 0.1$, demonstrating its robustness in strongly nonlinear regimes where perturbative approaches fail.

Conclusions—We have proposed in this Letter an extension of the strategy to construct trial states for DMRG-X, enabling the targeting of collective excitations in Josephson junction arrays. This approach allows for fully nonperturbative computations without approximating the system Hamiltonian, while preserving the compact nature of the superconducting phase drop across each junction. We demonstrated that our method remains accurate even where perturbation theory fails, including the regime where quantum phase slips become prominent and the energy spectrum acquires a strong dependence on offset charges.

This approach opens the door to applying tensor network methods more broadly to superconducting circuits with many degrees of freedom. In particular, it provides quantitatively reliable access to chain mode dynamics in

Josephson junction arrays, which may prove instrumental for future quantum information applications that seek to harness these modes as active resources.

Acknowledgment—The authors thank Agustin Di Paolo, Serge Florens, Marco Genoni, Salim Miklass, Felix Rautschke, and Pierre Rouchon for stimulating discussions. Numerical simulations were performed on the CLEPS cluster at INRIA and relied on the Julia programming language [62] and the packages `ITensors.jl` [63] and `KrylovKit.jl` [49].

* emilio.rui@alice-bob.com

§ These authors co-supervised the project.

- [1] N. A. Masluk, I. M. Pop, A. Kamal, Z. K. Mineev, and M. H. Devoret, *Physical Review Letters* **109**, [10.1103/physrevlett.109.137002](https://doi.org/10.1103/physrevlett.109.137002) (2012).
- [2] V. E. Manucharyan, N. A. Masluk, A. Kamal, J. Koch, L. I. Glazman, and M. H. Devoret, *Physical Review B* **85**, [10.1103/physrevb.85.024521](https://doi.org/10.1103/physrevb.85.024521) (2012).
- [3] A. Gyenis, P. S. Mundada, A. Di Paolo, T. M. Hazard, X. You, D. I. Schuster, J. Koch, A. Blais, and A. A. Houck, *PRX Quantum* **2**, [10.1103/prxquantum.2.010339](https://doi.org/10.1103/prxquantum.2.010339) (2021).
- [4] W. C. Smith, A. Kou, X. Xiao, U. Vool, and M. H. Devoret, *npj Quantum Inf.* **6**, 1 (2020).
- [5] W. C. Smith, M. Villiers, A. Marquet, J. Palomo, M. R. Delbecq, T. Kontos, P. Campagne-Ibarcq, B. Douçot, and Z. Leghtas, *Phys. Rev. X* **12**, 021002 (2022).
- [6] R. Lescanne, M. Villiers, T. Peronnin, A. Sarlette, M. Delbecq, B. Huard, T. Kontos, M. Mirrahimi, and Z. Leghtas, *Nature Physics* **16**, 509 (2020).
- [7] U. Réglade, A. Bocquet, R. Gautier, A. Marquet, E. Albertinale, N. Pankratova, M. Hallén, F. Rautschke, L.-A. Sellem, P. Rouchon, A. Sarlette, M. Mirrahimi, P. Campagne-Ibarcq, R. Lescanne, S. Jezouin, and Z. Leghtas, *Quantum control of a cat-qubit with bit-flip times exceeding ten seconds* (2023).
- [8] M. T. Bell, I. A. Sadovskyy, L. B. Ioffe, A. Yu. Kitaev, and M. E. Gershenson, *Phys. Rev. Lett.* **109**, 137003 (2012).
- [9] N. Crescini, S. Cailleaux, W. Guichard, C. Naud, O. Buisson, K. W. Murch, and N. Roch, *Nat. Phys.* **19**, 851 (2023).
- [10] B. Ho Eom, P. K. Day, H. G. LeDuc, and J. Zmuidzinas, *Nature Physics* **8**, 623–627 (2012).
- [11] C. Macklin, K. O’Brien, D. Hover, M. E. Schwartz, V. Bolkhovskiy, X. Zhang, W. D. Oliver, and I. Siddiqi, *Science* **350**, 307–310 (2015).
- [12] N. Roch, E. Flurin, F. Nguyen, P. Morfin, P. Campagne-Ibarcq, M. H. Devoret, and B. Huard, *Physical Review Letters* **108**, [10.1103/physrevlett.108.147701](https://doi.org/10.1103/physrevlett.108.147701) (2012).
- [13] D. G. Ferguson, A. A. Houck, and J. Koch, *Physical Review X* **3**, [10.1103/physrevx.3.011003](https://doi.org/10.1103/physrevx.3.011003) (2013).
- [14] G. Viola and G. Catelani, *Physical Review B* **92**, [10.1103/physrevb.92.224511](https://doi.org/10.1103/physrevb.92.224511) (2015).
- [15] S. Sorokanich, M. Hays, and N. C. Warrington, *Exact and approximate fluxonium array modes* (2024).
- [16] T. Weißl, B. Küng, E. Dumur, A. K. Feofanov, I. Matei, C. Naud, O. Buisson, F. W. J. Hekking,

- and W. Guichard, *Physical Review B* **92**, [10.1103/physrevb.92.104508](https://doi.org/10.1103/physrevb.92.104508) (2015).
- [17] S. Singh, G. Refael, A. Clerk, and E. Rosenfeld, *Impact of Josephson junction array modes on fluxonium readout* (2024).
- [18] S. R. White, *Physical Review Letters* **69**, 2863 (1992).
- [19] U. Schollwöck, *Annals of Physics* **326**, 96–192 (2011).
- [20] G. Vidal, *Physical Review Letters* **91**, [10.1103/physrevlett.91.147902](https://doi.org/10.1103/physrevlett.91.147902) (2003).
- [21] S. Paeckel, T. Köhler, A. Swoboda, S. R. Manmana, U. Schollwöck, and C. Hubig, *Annals of Physics* **411**, 167998 (2019).
- [22] A. Di Paolo, T. E. Baker, A. Foley, D. Sénéchal, and A. Blais, *npj Quantum Information* **7**, 11 (2021).
- [23] T. E. Baker, Block lanczos method for excited states on a quantum computer (2021), [arXiv:2109.14114](https://arxiv.org/abs/2109.14114).
- [24] V. Khemani, F. Pollmann, and S. Sondhi, *Physical Review Letters* **116**, [10.1103/physrevlett.116.247204](https://doi.org/10.1103/physrevlett.116.247204) (2016).
- [25] C. Berke, E. Varvelis, S. Trebst, A. Altland, and D. P. DiVincenzo, *Nature Communications* **13**, [10.1038/s41467-022-29940-y](https://doi.org/10.1038/s41467-022-29940-y) (2022).
- [26] S.-D. Börner, C. Berke, D. P. DiVincenzo, S. Trebst, and A. Altland, *Phys. Rev. Res.* **6**, 033128 (2024).
- [27] E. Rui, Master’s thesis, University of Milan (2023) https://minerva.unimi.it/permalink/39UMI_INST/16hmm17/alma991017855100706031.
- [28] H. Putterman, K. Noh, C. T. Hann, G. S. MacCabe, S. Aghaeimeibodi, R. N. Patel, M. Lee, W. M. Jones, H. Moradinejad, R. Rodriguez, N. Mahuli, J. Rose, J. C. Owens, H. Levine, E. Rosenfeld, P. Reinhold, L. Monceli, J. A. Alcid, N. Alidoust, P. Arrangoiz-Arriola, J. Barnett, P. Bienias, H. A. Carson, C. Chen, L. Chen, H. Chinkezzian, E. M. Chisholm, M.-H. Chou, A. Clerk, A. Clifford, R. Cosmic, A. V. Curiel, E. Davis, L. DeLorenzo, J. M. D’Ewart, A. Diky, N. D’Souza, P. T. Dumitrescu, S. Eisenmann, E. Elkhoully, G. Evenbly, M. T. Fang, Y. Fang, M. J. Fling, W. Fon, G. Garcia, A. V. Gorshkov, J. A. Grant, M. J. Gray, S. Grimberg, A. L. Grimsmo, A. Haim, J. Hand, Y. He, M. Hernandez, D. Hover, J. S. C. Hung, M. Hunt, J. Iverson, I. Jarrige, J.-C. Jaskula, L. Jiang, M. Kalae, R. Karabalin, P. J. Karalekas, A. J. Keller, A. Khalajhedayati, A. Kubica, H. Lee, C. Leroux, S. Lieu, V. Ly, K. V. Madrigal, G. Marcaud, G. McCabe, C. Miles, A. Milsted, J. Minguzzi, A. Mishra, B. Mukherjee, M. Naghiloo, E. Oblepias, G. Ortuno, J. Pagdilao, N. Pancotti, A. Panduro, J. Paquette, M. Park, G. A. Peairs, D. Perello, E. C. Peterson, S. Ponte, J. Preskill, J. Qiao, G. Refael, R. Resnick, A. Retzker, O. A. Reyna, M. Runyan, C. A. Ryan, A. Sahnoud, E. Sanchez, R. Sanil, K. Sankar, Y. Sato, T. Scaffidi, S. Siavoshi, P. Sivarajah, T. Skogland, C.-J. Su, L. J. Swenson, S. M. Teo, A. Tomada, G. Torlai, E. A. Wollack, Y. Ye, J. A. Zerrudo, K. Zhang, F. G. S. L. Brandão, M. H. Matheny, and O. Painter, *Nature* **638**, 927–934 (2025).
- [29] F. Lange, L. Heunisch, H. Fehske, D. P. DiVincenzo, and M. J. Hartmann, *Cross-talk in superconducting qubit lattices with tunable couplers - comparing transmon and fluxonium architectures* (2025).
- [30] S. González-García, A. Szasz, A. Pagano, D. Kafri, G. Vidal, and A. Di Paolo, [arXiv 10.48550/arXiv.2506.24109](https://arxiv.org/abs/10.48550/arXiv.2506.24109) (2025), [2506.24109](https://arxiv.org/abs/2506.24109).
- [31] S. E. Nigg, H. Paik, B. Vlastakis, G. Kirchmair, S. Shankar, L. Frunzio, M. H. Devoret, R. J. Schoelkopf, and S. M. Girvin, *Physical Review Letters* **108**, [10.1103/physrevlett.108.240502](https://doi.org/10.1103/physrevlett.108.240502) (2012).
- [32] Z. K. Mineev, Z. Leghtas, S. O. Mundhada, L. Christakis, I. M. Pop, and M. H. Devoret, Energy-participation quantization of Josephson circuits (2020), [arXiv:2010.00620](https://arxiv.org/abs/2010.00620).
- [33] B. Blain, G. Marchegiani, L. Amico, and G. Catelani, *Suppressing chaos with mixed superconducting qubit devices* (2024).
- [34] K. A. Matveev, A. I. Larkin, and L. I. Glazman, *Physical Review Letters* **89**, [10.1103/physrevlett.89.096802](https://doi.org/10.1103/physrevlett.89.096802) (2002).
- [35] I. M. Pop, I. Protopopov, F. Lecocq, Z. Peng, B. Pannetier, O. Buisson, and W. Guichard, *Nat. Phys.* **6**, 589 (2010).
- [36] J. Koch, T. M. Yu, J. Gambetta, A. A. Houck, D. I. Schuster, J. Majer, A. Blais, M. H. Devoret, S. M. Girvin, and R. J. Schoelkopf, *Physical Review A* **76**, [10.1103/physreva.76.042319](https://doi.org/10.1103/physreva.76.042319) (2007).
- [37] See Supplementary Material for details which includes Refs.[64–76].
- [38] M. Debertolis, I. Snyman, and S. Florens, *Physical Review B* **106**, [10.1103/physrevb.106.125115](https://doi.org/10.1103/physrevb.106.125115) (2022).
- [39] M. Debertolis, *Natural super-orbitals representation of many-body operators* (2025).
- [40] Y. Núñez-Fernández, M. Debertolis, and S. Florens, *Resolving space-time structures of quantum impurities with a numerically-exact algorithm using few-body revealing* (2025).
- [41] J. Williamson, *American Journal of Mathematics* **58**, 141 (1936).
- [42] J. Colpa, *Physica A: Statistical Mechanics and its Applications* **93**, 327–353 (1978).
- [43] M. G. Genoni, L. Lami, and A. Serafini, *Contemporary Physics* **57**, 331–349 (2016).
- [44] A. Serafini, *Quantum Continuous Variables* (CRC Press, 2017).
- [45] A. Petrescu, H. E. Türeci, A. V. Ustinov, and I. M. Pop, *Physical Review B* **98**, [10.1103/physrevb.98.174505](https://doi.org/10.1103/physrevb.98.174505) (2018).
- [46] A. Petrescu, C. Le Calonnec, C. Leroux, A. Di Paolo, P. Mundada, S. Sussman, A. Vrajitoarea, A. A. Houck, and A. Blais, *Physical Review Applied* **19**, [10.1103/physrevapplied.19.044003](https://doi.org/10.1103/physrevapplied.19.044003) (2023).
- [47] X. Yu, D. Pekker, and B. K. Clark, *Physical Review Letters* **118**, [10.1103/physrevlett.118.017201](https://doi.org/10.1103/physrevlett.118.017201) (2017).
- [48] A. Baiardi, A. K. Kelemen, and M. Reiher, *Journal of Chemical Theory and Computation* **18**, 415–430 (2021).
- [49] J. Haegeman, *Krylovkit* (2025).
- [50] E. Rui, A. Petrescu, and J. Cohen, in preparation (2025).
- [51] M. Lee, M.-S. Choi, and M. Y. Choi, *Physical Review B* **68**, [10.1103/physrevb.68.144506](https://doi.org/10.1103/physrevb.68.144506) (2003).
- [52] D. K. Weiss, A. C. Y. Li, D. G. Ferguson, and J. Koch, *Physical Review B* **100**, [10.1103/physrevb.100.224507](https://doi.org/10.1103/physrevb.100.224507) (2019).
- [53] K. Kaur, T. Sépulcre, N. Roch, I. Snyman, S. Florens, and S. Bera, *Physical Review Letters* **127**, [10.1103/physrevlett.127.237702](https://doi.org/10.1103/physrevlett.127.237702) (2021).
- [54] I. M. Pop, B. Douçot, L. Ioffe, I. Protopopov, F. Lecocq, I. Matei, O. Buisson, and W. Guichard, *Physical Review B* **85**, [10.1103/physrevb.85.094503](https://doi.org/10.1103/physrevb.85.094503) (2012).
- [55] J. R. Friedman and D. V. Averin, *Physical Review Letters* **88**, [10.1103/physrevlett.88.050403](https://doi.org/10.1103/physrevlett.88.050403) (2002).

- [56] M. Bell, W. Zhang, L. Ioffe, and M. Gershenson, *Physical Review Letters* **116**, [10.1103/physrevlett.116.107002](https://doi.org/10.1103/physrevlett.116.107002) (2016).
- [57] J. E. Mooij and C. J. P. M. Harmans, *New Journal of Physics* **7**, 219–219 (2005).
- [58] J. E. Mooij and Y. V. Nazarov, *Nature Physics* **2**, 169–172 (2006).
- [59] A. M. Hriscu and Y. V. Nazarov, *Physical Review B* **83**, [10.1103/physrevb.83.174511](https://doi.org/10.1103/physrevb.83.174511) (2011).
- [60] G. Rastelli, I. M. Pop, and F. W. J. Hekking, *Physical Review B* **87**, [10.1103/physrevb.87.174513](https://doi.org/10.1103/physrevb.87.174513) (2013).
- [61] V. Manucharian, *Superinductance*, Ph.d. thesis, Yale University (2012).
- [62] J. Bezanson, A. Edelman, S. Karpinski, and V. B. Shah, *SIAM review* **59**, 65 (2017).
- [63] M. Fishman, S. R. White, and E. M. Stoudenmire, *SciPost Phys. Codebases* , 4 (2022).
- [64] D. Ding, H.-S. Ku, Y. Shi, and H.-H. Zhao, *Physical Review B* **103**, [10.1103/physrevb.103.174501](https://doi.org/10.1103/physrevb.103.174501) (2021).
- [65] U. Vool and M. Devoret, *International Journal of Circuit Theory and Applications* **45**, 897 (2017).
- [66] U. Schollwöck, *Reviews of Modern Physics* **77**, 259–315 (2005).
- [67] U. Schollwöck, *Annals of Physics* **326**, 96–192 (2011).
- [68] J. C. Bridgeman and C. T. Chubb, *Journal of Physics A: Mathematical and Theoretical* **50**, 223001 (2017).
- [69] R. Orús, *Annals of Physics* **349**, 117–158 (2014).
- [70] C. Hubig, J. Haegeman, and U. Schollwöck, *Physical Review B* **97**, [10.1103/physrevb.97.045125](https://doi.org/10.1103/physrevb.97.045125) (2018).
- [71] S. R. White, *Physical Review B* **72**, [10.1103/physrevb.72.180403](https://doi.org/10.1103/physrevb.72.180403) (2005).
- [72] D. E. Parker, X. Cao, and M. P. Zaletel, *Physical Review B* **102**, [10.1103/physrevb.102.035147](https://doi.org/10.1103/physrevb.102.035147) (2020).
- [73] G. Citeroni, M. Polini, M. Dapolito, D. N. Basov, and G. Mazza, *Ultrafast dynamics of quantum matter driven by time-energy entangled photons* (2025).
- [74] G. Zhu, D. G. Ferguson, V. E. Manucharyan, and J. Koch, *Physical Review B* **87**, [10.1103/physrevb.87.024510](https://doi.org/10.1103/physrevb.87.024510) (2013).
- [75] F. Yilmaz, S. Singh, M. F. S. Zwanenburg, J. Hu, T. V. Stefanski, and C. K. Andersen, *Energy participation ratio analysis for very anharmonic superconducting circuits* (2024).
- [76] J. Cohen, A. Petrescu, R. Shillito, and A. Blais, *PRX Quantum* **4**, [10.1103/prxquantum.4.020312](https://doi.org/10.1103/prxquantum.4.020312) (2023).

SUPPLEMENTARY MATERIAL

Tensor Network representation of excitations in Josephson junction arrays

Emilio Rui,^{1,2,*} Joachim Cohen,^{1,§} and Alexandru Petrescu^{2,§}

¹*Alice and Bob, 53 Bd du Général Martial Valin, 75015 Paris, France*

²*Laboratoire de Physique de l'École Normale Supérieure,
École Normale Supérieure, Centre Automatique et Systèmes,
Mines Paris, Université PSL, CNRS, Inria, Paris, France*

(Dated: October 13, 2025)

The Supplementary Material is structured as follows. In Sec. I we derive the Hamiltonian of the system under study, following Ref. [1]. In Sec. II we introduce the tensor-network formalism and show how to efficiently represent the Hamiltonian in matrix-product form. In Sec. III we derive the normal-mode bosonic operators from the linearized Hamiltonian. In Sec. IV we incorporate the nonlinearity of the junctions in the array and present the perturbative computation of cross-Kerr interactions between the array modes. In Sec. V we develop the perturbation theory for the fluxonium qubit, labeled ‘‘Pert. II’’ in the main text. While the approach is not fundamentally different from previous treatments [2, 3], we formulate it in a way that facilitates numerical implementation, and validate it with an alternative parameter set in Fig. S1.

I. SUPERINDUCTANCE HAMILTONIAN

In this section we derive the Hamiltonian of the system shown in Fig. 1 of the main text. The derivation follows Ref. [1] with the only difference that we explicitly perform a free-mode removal [4], which makes the analysis applicable also to nonuniform junction arrays. This refinement is marginal and is included here mainly for completeness. The same derivation reduces to a purely linear LC oscillator upon setting $E_J^b = 0$. The Lagrangian describing the circuit[5] in Fig. 1 of the main text is

$$\begin{aligned}
 L(\Phi, \dot{\Phi}) = & \frac{e^2}{4} \sum_{i=0}^{N_J} \frac{(\dot{\Phi}_i - \dot{\Phi}_{i-1})^2}{E_C^a} + \frac{e^2}{4} \frac{(\dot{\Phi}_0 - \dot{\Phi}_{N_J})^2}{E_C^b} \\
 & + \frac{e^2}{4} \left(\sum_{i=1}^{N_J-1} \frac{\dot{\Phi}_i^2}{E_g^a} + \frac{\dot{\Phi}_0^2}{E_g^{b,0}} + \frac{\dot{\Phi}_{N_J}^2}{E_g^{b,N_J}} \right) \\
 & + \sum_{i=1}^{N_J} E_{J,i}^a \cos \left[\frac{2\pi}{\Phi_0} (\Phi_i - \Phi_{i-1}) \right] \\
 & + E_J^b \cos \left[\frac{2\pi}{\Phi_0} (\Phi_{N_J} - \Phi_0 + \Phi_{\text{ext}}) \right],
 \end{aligned} \tag{S1}$$

where we have defined $\Phi = (\Phi_0, \dots, \Phi_{N_J})^\top$ as the vector of node fluxes, with $\Phi_0 = h/2e$ the superconducting flux quantum. $E_{J,i}^a$ are the Josephson energies of the large junctions in the array, and E_J^b is the Josephson energy of the small black-sheep junction. E_C^a and E_C^b denote the charging energies of the array junctions and the black-sheep junction, respectively, while E_g^a corresponds to the capacitance to ground in the array. Asymmetries in the capacitance to ground at the boundary islands, $E_g^{b,0}$ and E_g^{b,N_J} , are also included, accounting for possible asymmetric coupling to external circuitry [2].

We adopt the basis $\Theta_\Sigma = (\Sigma, \Theta_1, \dots, \Theta_{N_J})^\top$, where $\Theta_i = \Phi_i - \Phi_{i+1}$ denotes the branch flux across the i^{th} junction of the array, and $\Sigma = \sum_{i=0}^{N_J} \Phi_i$ is the collective sum coordinate. In this representation, the sum mode Σ appears as a free mode; however, it remains capacitively coupled to the array degrees of freedom. Following Ref. [4], we eliminate Σ to obtain a reduced description of the system.

The capacitance matrix is transformed as $\mathbf{C}_\Theta = (\mathbf{R}^T)^{-1} \mathbf{C}_\Phi \mathbf{R}^{-1}$ where \mathbf{R} is the coordinate transformation such that $\Theta_\Sigma = \mathbf{R}\Phi$, by representing it in block form

$$\mathbf{C}_\Theta = \begin{pmatrix} \mathbf{C}_{\Sigma\Sigma} & \mathbf{C}_{\Sigma\theta} \\ \mathbf{C}_{\Sigma\theta}^\top & \mathbf{C}_{\theta\theta} \end{pmatrix}, \tag{S2}$$

we aim to eliminate the off-diagonal blocks, where $C_{\theta\theta}$ is the $N_J \times N_J$ submatrix corresponding to the junction coordinates, and $C_{\Sigma\Sigma}$ is the 1×1 block corresponding to the sum mode. We now define the transformed coordinates

$$\Theta'_\Sigma = W \Theta_\Sigma = (\Sigma', \Theta_1, \dots, \Theta_{N_J})^\top, \tag{S3}$$

such that the mode Σ' is decoupled from the dynamics. The transformation matrix W that achieves this is [2, 6]

$$(W^\top)^{-1} = \begin{pmatrix} 1 & \mathbf{0} \\ -\mathbf{C}_{\Sigma\theta}^\top \mathbf{C}_{\Sigma\Sigma}^{-1} & \mathbf{I}_{N_J} \end{pmatrix}. \tag{S4}$$

The reduced capacitance matrix \mathbf{C} , excluding the decoupled free mode Σ' , is then the bottom-right $N_J \times N_J$ block of

$$\mathbf{C}' = (W^\top)^{-1} \mathbf{C}_\Theta W^{-1} = \begin{pmatrix} \mathbf{C}_{\Sigma'\Sigma'} & \mathbf{0} \\ \mathbf{0} & \mathbf{C} \end{pmatrix}. \tag{S5}$$

By denoting $\Theta = (\Theta_1, \dots, \Theta_{N_J})^\top$ the reduced variables (neglecting the uncoupled mode), the Lagrangian

* emilio.rui@alice-bob.com

§ These authors co-supervised the project.

of the system is

$$L(\Theta, \dot{\Theta}) = \frac{1}{2} \dot{\Theta}^\top \mathbf{C} \dot{\Theta} + \sum_{i=1}^{N_J} E_{J,i}^a \cos\left(2\pi \frac{\Theta_i}{\Phi_0}\right) + E_J^b \cos\left[\frac{2\pi}{\Phi_0} \left(\sum_{i=1}^{N_J} \Theta_i + \Phi_{\text{ext}}\right)\right]. \quad (\text{S6})$$

A Legendre transform yields the Hamiltonian

$$H = \frac{1}{2} \mathbf{q}_\Theta^\top \mathbf{C}^{-1} \mathbf{q}_\Theta - \sum_{i=1}^{N_J} E_{J,i}^a \cos \theta_i - E_J^b \cos\left(\sum_{i=1}^{N_J} \theta_i + \varphi_{\text{ext}}\right), \quad (\text{S7})$$

where $\theta_i = 2\pi\Theta_i/\Phi_0$ and $\varphi_{\text{ext}} = 2\pi\Phi_{\text{ext}}/\Phi_0$. By explicitly separating the diagonal part of the kinetic term and including gate charges $n_{g,i}$ in the array [1], the Hamiltonian (upon quantization) can be written as

$$\hat{H} = \sum_{i=1}^{N_J} \hat{H}_{0,i} + \sum_{i \neq j}^{N_J} \hbar g_{ij} (\hat{n}_i - n_{g,i})(\hat{n}_j - n_{g,j}) - E_J^b \cos\left(\sum_{i=1}^{N_J} \hat{\theta}_i + \varphi_{\text{ext}}\right), \quad (\text{S8})$$

where

$$\hat{H}_{0,i} = 4E_{C,i}(\hat{n}_i - n_{g,i})^2 - E_{J,i}^a \cos \hat{\theta}_i, \quad (\text{S9})$$

$$E_{C,i} = \frac{e^2}{2} [\mathbf{C}_\Theta^{-1}]_{ii}, \quad (\text{S10})$$

$$g_{ij} = 2e^2 [\mathbf{C}_\Theta^{-1}]_{ij}. \quad (\text{S11})$$

This, upon quantization, gives our starting point Hamiltonian. Below, we discuss how this can be represented as a matrix-product operator.

II. MPO REPRESENTATION OF JJ ARRAY HAMILTONIAN

In this appendix, we explicitly show how to efficiently represent the Hamiltonian of junction arrays in matrix-product operator (MPO) form. We first give a brief overview of the matrix product state/operator framework, and then analyze the bond dimension of each term in the Hamiltonian. Our analysis demonstrates that, despite the presence of long-range and nonlinear couplings, the Hamiltonian admits an MPO representation whose bond dimension scales only polynomially with the system size. Furthermore, by allowing for small truncation errors, the representation can be compressed to a constant bond dimension.

A generic quantum state of an N -body system with local basis $\{|s_i\rangle\}$ can be represented as a matrix-product state (MPS) [7–11]

$$|\psi\rangle = \sum_{s_i=0}^{d-1} \sum_{a_i=1}^D M_{a_1}^{(1),s_1} M_{a_1,a_2}^{(2),s_2} \dots M_{a_{N-1}}^{(N),s_N} |s_1 s_2 \dots s_N\rangle \quad (\text{S12})$$

where each probability amplitude is expressed as a product of matrices $M^{(i),s_i}$. This representation requires to store $O(dND^2)$ elements, where d is the local Hilbert space dimension, and D is what is called the bond dimension. The bond dimension scales with the entanglement of the quantum state [9, 12], making tensor networks particularly efficient at compressing low-entanglement, localized quantum states. Throughout this work we allowed for maximum bond dimensions of $D = 250$. This formalism can be extended to represent operators in the form of MPOs

$$\hat{O} = \sum_{s_i, s'_i=0}^{d-1} \sum_{a_i=1}^D M_{a_1}^{(1),s_1,s'_1} M_{a_1,a_2}^{(2),s_2,s'_2} \dots \quad (\text{S13})$$

$$\dots M_{a_{N-1}}^{(N),s_N,s'_N} |s'_1 s'_2 \dots s'_N\rangle \langle s_1 s_2 \dots s_N| \quad (\text{S14})$$

by adding an extra set of indices s'_i . The storage cost for an MPO scales as $O(d^2ND^2)$. As in the MPS case, efficiency depends on how the bond dimension D grows with system size, which is associated again with the locality of the interactions described by \hat{O} . The multidimensional tensor $M_{a_{i-1}a_i}^{(i),s_i,s'_i}$ denotes a matrix of size $D \times D$ whose entries are local operators acting on the i^{th} system of size $d \times d$ [13]

In our system, we work in the energy eigenbasis of the local Hamiltonian $\hat{H}_{0,i}$ introduced in Eq. (2) of the main text. The number of quantum systems is thus given by the number of junctions in the array, $N = N_J$, while the local Hilbert-space dimension d is determined by the number of eigenstates retained for each junction. To construct this basis, we diagonalize $\hat{H}_{0,i}$ in the local charge basis [14] and keep the $d = 8$ lowest-energy eigenstates,

$$\{|s_i\rangle \equiv |\psi_{s_i}^{(i)}\rangle \mid s_i = 0, \dots, d-1\}.$$

To represent Eq. (S8) as an MPO, we use the fact that the sum of two MPOs is itself an MPO, with bond dimension equal to the sum of the individual bond dimensions. This allows us to analyze each term of the Hamiltonian independently. The first term of Eq. (S8) is a sum of on-site operators and can be represented as an MPO of bond dimension $D = 2$ [13]

$$\sum_{i=1}^{N_J} \hat{H}_{0,i} = (\hat{H}_{0,1} \ \mathbb{I}) \otimes \begin{pmatrix} \mathbb{I} & 0 \\ \hat{H}_{0,2} & \mathbb{I} \end{pmatrix} \otimes \dots \otimes \begin{pmatrix} \mathbb{I} & \\ & \hat{H}_{0,N_J} \end{pmatrix}. \quad (\text{S15})$$

The second term of Eq. (S8) represents an all-to-all two-body coupling. It can be expressed as an MPO of

bond dimension $D = 2N$ [13] by factorizing

$$\sum_{i,j=1}^{N_J} g_{ij} \hat{n}_i \hat{n}_j = \sum_{i=1}^{N_J} \hat{n}_i \left(\sum_{j=1}^{N_J} g_{ij} \hat{n}_j \right). \quad (\text{S16})$$

The term $\sum_j g_{ij} \hat{n}_j$ is itself a sum of local operators and can be represented with bond dimension $D = 2$. Since the product of two MPOs has bond dimension equal to the product of their bond dimensions [13], and each \hat{n}_i can be represented as an MPO with $D = 1$

$$\hat{n}_i = (\mathbb{I}) \otimes \cdots \otimes (\hat{n}_i) \otimes \cdots \otimes (\mathbb{I}). \quad (\text{S17})$$

We obtain an overall bond dimension $D = 2N_J$ before compression. By applying standard MPO compression techniques [15, 16], this value can be further reduced. For all parameter choices considered, we find that after minor truncations—comparable to machine precision—the bond dimension of the charge-coupling term is $D = 5$. We emphasize that the foregoing analysis remains valid in the presence of charge offsets, since their inclusion simply amounts to the substitution $\hat{n}_i \rightarrow \hat{n}_i - n_{g,i}$ in the preceding expressions.

The last term of Eq. (S8) is the cosine associated with the black-sheep junction, which also represents an all-to-all coupling. It can be expressed as

$$\cos \left(\sum_{j=1}^{N_J} \hat{\theta}_j \right) = \frac{e^{i \sum_{j=1}^{N_J} \hat{\theta}_j} + e^{-i \sum_{j=1}^{N_J} \hat{\theta}_j}}{2}. \quad (\text{S18})$$

Since

$$e^{i \sum_{j=1}^{N_J} \hat{\theta}_j} = \left(e^{i \hat{\theta}_1} \right) \otimes \cdots \otimes \left(e^{i \hat{\theta}_j} \right) \otimes \cdots \otimes \left(e^{i \hat{\theta}_{N_J}} \right), \quad (\text{S19})$$

is already a tensor product, it is directly an MPO with bond dimension $D = 1$. Thus, the cosine—without expanding the exponential—is an MPO with $D = 2$. This property remains valid for any cosine of a linear combination of local operators, such as those appearing in the BBQ formalism [17–19].

III. MPO REPRESENTATION OF NORMAL MODE BOSONIC OPERATORS

In this section, we discuss how to obtain the bosonic operators of the array normal modes, and how to express them as MPOs. The linearized Hamiltonian of Eq. (S8), neglecting the black-sheep junction, is

$$\hat{H}_{\text{lin}} = \sum_{i=1}^{N_J} \left(4E_{C,i} \hat{n}_i^2 + \frac{\tilde{E}_{J,i}^a}{2} \hat{\theta}_i^2 \right) + \sum_{i,j=1}^{N_J} g_{ij} \hat{n}_i \hat{n}_j, \quad (\text{S20})$$

where we introduced the renormalized Josephson energy

$$\tilde{E}_{J,k}^a = e^{-\eta_k/4} E_{J,k}^a, \quad (\text{S21})$$

with η_k a correction factor associated with the normal ordering of the cosine potential [20] determined by the transcendental equation

$$e^{-\eta_k/4} \eta_k^2 = \frac{8E_{C,k}}{E_J^k}. \quad (\text{S22})$$

Equation (S20) is quadratic, therefore diagonalizable via a symplectic transformation $S_{\xi\theta}$ [21–25]. We define $\hat{\mathbf{r}}_\theta$ and $\hat{\mathbf{r}}_\xi$ as the vectors of local and normal-mode canonical variables, respectively:

$$\hat{\mathbf{r}}_\theta = (\hat{\theta}_1, \dots, \hat{\theta}_{N_J}, \hat{n}_1, \dots, \hat{n}_{N_J})^\top, \quad (\text{1a})$$

$$\hat{\mathbf{r}}_\xi = (\hat{\xi}_0, \dots, \hat{\xi}_{N_J-1}, \hat{n}_{\xi,1}, \dots, \hat{n}_{\xi,N_J-1})^\top = S_{\xi\theta} \hat{\mathbf{r}}_\theta. \quad (\text{1b})$$

In terms of these variables, the quadratic Hamiltonian reads

$$\begin{aligned} H_{\text{lin}} &= \frac{1}{2} \hat{\mathbf{r}}_\xi^\top D \hat{\mathbf{r}}_\xi = \sum_{j=0}^{N_J-1} \frac{\omega_j}{2} \left(\hat{\xi}_j^2 + \hat{n}_{\xi,j}^2 \right) \\ &= \sum_{j=0}^{N_J-1} \omega_j \left(\hat{A}_j^\dagger \hat{A}_j + \frac{1}{2} \right), \end{aligned} \quad (\text{S24})$$

where the normal-mode bosonic operators are defined as

$$\hat{A}_j = \frac{1}{\sqrt{2}} \left(\hat{\xi}_j + i \hat{n}_j \right). \quad (\text{S25})$$

By defining the local bosonic operators as

$$\hat{b}_k = \frac{\hat{\theta}_k}{\sqrt{2\eta_k}} + i \sqrt{\frac{\eta_k}{2}} \hat{n}_k, \quad (\text{S26})$$

we can collect the bosonic operators into vectors of normal modes and local modes,

$$\hat{\mathbf{A}} = (\hat{A}_1, \dots, \hat{A}_{N_J}, \hat{A}_1^\dagger, \dots, \hat{A}_{N_J}^\dagger)^\top = T_1 \hat{\mathbf{r}}_\xi, \quad (\text{a})$$

$$\hat{\mathbf{b}} = (\hat{b}_1, \dots, \hat{b}_{N_J}, \hat{b}_1^\dagger, \dots, \hat{b}_{N_J}^\dagger)^\top = T_2 \hat{\mathbf{r}}_\theta. \quad (\text{b})$$

We obtain eventually the desired linear transformation between normal mode bosonic operators and local ones

$$\hat{\mathbf{A}} = T_1^{-1} S_{\xi\theta} T_2 \hat{\mathbf{b}}, \quad (\text{S28})$$

where T_1 and T_2 denote the respective transformations between bosonic and canonical variables.

In order to express the normal mode bosonic operators \hat{b}_i as ladder operators in the local eigenbasis used to represent the Hamiltonian Sec. II,

$$\hat{b}_i \approx \sum_{k=1}^{d-1} \sqrt{k} |\psi_{k-1}^{(i)}\rangle \langle \psi_k^{(i)}|. \quad (\text{S29})$$

Since the normal-mode operators \hat{A}_k are linear combinations of the local operators, they can also be written as MPOs with bond dimension $D_A = 2$. Trial states are obtained by applying these MPOs to a reference state $|\Psi_0\rangle$. Applying an MPO to an MPS produces another MPS with bond dimension equal to the product of the two; hence, if the reference state $|\Psi_0\rangle$ is well represented by a low-bond-dimension MPS [1], each created excitation increases the bond dimension only mildly, enabling the practical use of the DMRG-X algorithm.

IV. CROSS-KERR BETWEEN CHAIN MODES IN AN SUPERINDUCTOR

We now use the linearized analysis in Sec. III to compute cross-Kerr nonlinearities in a superinductor associated with the nonlinearity of the array using the black-box quantization approach [18–20, 26], as shown in Fig. 1 of the main text. The superinductor Hamiltonian Eq. (S8) (with no black-sheep junction involved) can be separated into a linear part Eq. (S20) and a nonlinear part

$$\begin{aligned} \hat{H} &= \hat{H}_{\text{lin}} + \hat{H}_{\text{nl}} \\ &= \sum_{i=1}^{N_J} \omega_i \hat{A}_i^\dagger \hat{A}_i - \sum_{j=1}^{N_J} E_{J,j}^a \left(\cos \hat{\theta}_j + \frac{e^{-\frac{\eta_j}{4}}}{2} \hat{\theta}_j^2 \right). \end{aligned} \quad (\text{S30})$$

The nonlinearity generates therefore self-Kerr and cross-Kerr terms between the normal modes of the array annihilated by the operators \hat{A}_i . When expressing the phase variables as linear combinations of the normal-mode bosonic operators $\hat{\theta}_j = \sum_k u_{jk} \hat{A}_k + u_{jk}^* \hat{A}_k^\dagger$, the cross- and self-Kerr coupling constants from first-order rotating-wave approximation [20] are

$$\chi_{jk}^{(1)} = -\frac{1}{4} \sum_{m=1}^{N_J} |u_{mj}|^2 |u_{mk}|^2 E_{J,m}^a, \quad (\text{S31})$$

which is defined in terms of Josephson energies renormalized by factors arising from normal ordering

$$E_{J,m}^a = e^{-\frac{1}{4} \sum_k |u_{mk}|^2} E_{J,m}^a. \quad (\text{S32})$$

We find that including these factors is crucial for the convergence of the highest-frequency chain modes. The induced nonuniformity of the Josephson energies $E_{J,m}^a$ lifts the degeneracy and localizes the highest frequency modes near the two boundaries. This localization has two consequences: first, DMRG-X fails to converge when trial states are constructed without accounting for it; second, the appearance of two distinct tails in the cross-Kerr spectrum of Fig. 1-b of the main text reflects the boundary localization of the modes, while their asymmetry arises from the unequal capacitances to ground at the two ends of the array as listed in Table 1 of the main text.

Before concluding this section, we note that in certain cases the calculation can be made more precise by properly accounting for residual quadratic terms that appear in the normal-ordered expansion of the array nonlinearity. To see this, note that, due to the canonical transformation, the quadratic terms in Eq. (S30) do not fully cancel. They amount to a residual quadratic part of the Hamiltonian.

$$\begin{aligned} \hat{H}_{\text{lin,res}} &= \\ &= \sum_{j=1}^{N_J} \frac{E_{J,j}^a}{2} \left(e^{-\frac{\eta_j}{4}} - e^{-\frac{1}{2} \sum_k |u_{jk}|^2} \right) \left(\sum_k u_{jk} \hat{A}_k + u_{jk}^* \hat{A}_k^\dagger \right)^2. \end{aligned} \quad (\text{S33})$$

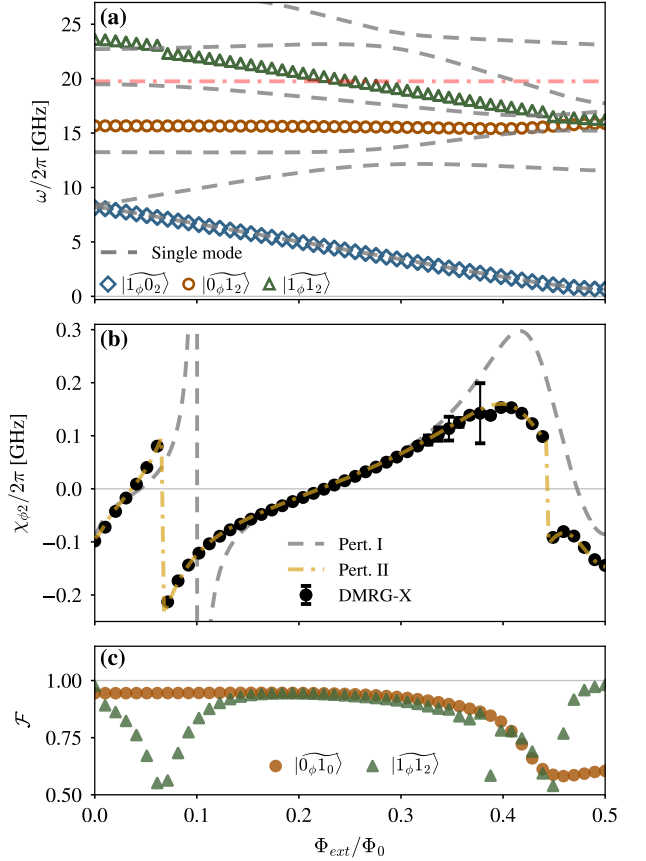


FIG. S1. DMRG-X analysis of a fluxonium circuit with $N_J = 95$ junctions in the superinductor (the circuit parameters are listed in Table S1). The analysis follows Fig. 2 of the main text, but for a longer and less nonlinear array. In panel (b), the cross-Kerr coupling $\chi_{\phi 2}$ exhibits a marked deviation from the first-order perturbative result (Pert. I), while showing improved agreement with the second-order perturbative approach (Pert. II) due to the weaker nonlinearity.

It is however possible to iteratively consider these linear contributions, by symplectically diagonalizing the quadratic Hamiltonian resulting from adding this residual part to the diagonal normal-mode Hamiltonian found above.

$$\tilde{H}_{\text{lin}} = \sum_k \omega_k^{(j)} \hat{A}_k^\dagger \hat{A}_k + H_{\text{lin,res}}. \quad (\text{S34})$$

For the parameter regimes considered, this step can be iterated and converges quickly to a set of normal-mode coefficients u_{jk}^∞ . In practice, the corrections are minor—below 0.1% in both mode frequencies and Kerr coefficients—and only marginally affect the quality of the trial states in DMRG-X simulations.

V. CROSS-KERR BETWEEN THE FLUXONIUM AND CHAIN MODES

In this appendix we introduce the perturbative approach labeled ‘‘Pert. II’’ in the main text. Based on Ref. [2], the method evaluates Kerr nonlinearities between the fluxonium mode and the array modes. Our treatment differs in that we perform numerically exact computations wherever possible and include frequency renormalizations from normal ordering of all bare modes. This leads to a clear improvement in precision when compared with exact numerics in the main text. We further validate the method in Fig. S1 using an alternative parameter set, listed in Table S1, corresponding to a fluxonium with a longer and less nonlinear array.

The nonlinearity caused by the array is significantly smaller than the one caused by the black sheep junction. Following [2] we therefore focus on the cross-Kerr caused only by the black sheep junction. Adding its term to the previous linearized Hamiltonian Eq. (S20), we have

$$\hat{H} = \hat{H}_{\text{lin}} - E_J^b \cos\left(\sum_{i=1}^{N_J} \hat{\theta}_i + \varphi_{\text{ext}}\right) \quad (\text{S35})$$

where we include the renormalization from normal-ordering as defined before in Eq. (S21). Due to the block structure of the linear part, the symplectic transformation diagonalizing it $S_{\xi\theta}$ does not mix phase and charge, that is

$$S_{\xi\theta} = \begin{pmatrix} C & 0 \\ 0 & (C^\top)^{-1} \end{pmatrix}. \quad (\text{S36})$$

This causes that normal mode phase variables ξ_j are linear combinations of only the junction phase drops θ_i . Importantly, the fundamental mode $\xi_0 \approx \sum_i \theta_i$, and therefore is the one mainly affected by the black-sheep nonlinearity. Following Ref. [2] we want to enforce exactly the equality by the defining a ‘‘fluxonium’’ phase variable $\phi = \sum_i \theta_i$, so to move the whole nonlinearity to the fundamental mode. We define the canonical variables

$$\hat{\mathbf{r}}_\phi = S_{\phi,\theta} \hat{\mathbf{r}} = (\hat{\phi}, \hat{\xi}_1, \dots, \hat{\xi}_{N_J-1}, \hat{n}_\phi, \hat{n}_{\xi_1}, \dots, \hat{n}_{\xi_{N_J-1}})^\top, \quad (\text{S37})$$

where the symplectic matrix has the same structure as before, $S_{\phi,\theta} = \text{diag}(B, (B^\top)^{-1})$, with B merely modifying the matrix A introduced above by replacing all entries on its top row with ones

$$B = \begin{bmatrix} 1 & 1 & \cdots & 1 \\ C_{2,1} & C_{2,2} & \cdots & C_{2,N_J} \\ \vdots & \vdots & \ddots & \vdots \\ C_{N_J,1} & C_{N_J,2} & \cdots & C_{N_J,N_J} \end{bmatrix} \quad (\text{S38})$$

In terms of the transformed variables, the full system Hamiltonian reads

$$\hat{H} = \hat{H}_\phi + \frac{1}{2} \hat{\mathbf{r}}_\xi^\top H_\xi \hat{\mathbf{r}}_\xi + \sum_j g_{\phi j}^{(n)} \hat{n}_\phi \hat{n}_{\xi j} + \sum_j g_{\phi j}^{(\varphi)} \hat{\phi} \hat{\xi}_j, \quad (\text{S39})$$

Set	N_J	E_J^a	E_C^a	E_J^b	E_C^b	E_g^a	$E_g^{b,0}$	E_g^{b,N_J}
4[2]	95	48.3	1.01	10.2	4.78	484	11.9	11.9

TABLE S1. Device parameters for the additional parameter set used in Fig. S1. All energies are in GHz.

where \mathbf{r}_ξ collects all normal-mode variables except the fluxonium ones $\hat{\phi}, \hat{n}_\phi$. Here, H_ξ is an $2(N_J-1) \times 2(N_J-1)$ matrix describing the residual couplings between chain modes; $g_{\phi j}^{(n)}$ denotes the capacitive coupling between the fluxonium and the j^{th} chain mode; and $g_{\phi j}^{(\varphi)}$ the corresponding flux coupling.

The fluxonium Hamiltonian itself, obtained by isolating the ϕ -mode charging and inductive terms from the transformed linearized Hamiltonian, is given by

$$\hat{H}_\phi = 4E_C^\phi \hat{n}_\phi^2 + \frac{E_L}{2} \hat{\phi}^2 - E_{Jb} \cos(\hat{\phi} + \varphi_{\text{ext}}). \quad (\text{S40})$$

Note that H_ξ is generally non-diagonal, as the change to \mathbf{r}_ϕ introduces off-diagonal terms determined by the circuit’s symmetries [2, 6].

We then symplectically diagonalize H_ξ , following the procedure outlined in Sec. III, to obtain dressed normal-mode bosonic operators for the array sector. This yields a star-coupling Hamiltonian in which the array modes couple only to the fluxonium mode,

$$\hat{H} = \hat{H}_\phi + \sum_k \left[\omega_k \hat{a}_k^\dagger \hat{a}_k + \hat{n}_\phi (\tilde{g}_{\phi k} \hat{a}_k + \text{h.c.}) \right], \quad (\text{S41})$$

where the effective couplings $\tilde{g}_{\phi k}$ now incorporate the normal-mode transformation. The Hamiltonian in Eq. (S41) thus describes a fluxonium mode linearly coupled to a set of harmonic oscillators (the array modes). Following [2, 27], one could apply perturbation theory to estimate the resulting cross-Kerr nonlinearities between the fluxonium and the array modes. Around resonances, an approach that agrees better with full numerics, however, is to restrict to a reduced subsystem consisting of the fluxonium and a single array mode [28], i.e., retaining only one term in the sum of Eq. (S41). For the chosen k^{th} mode, the cross-Kerr $\chi_{\phi k}$ can then be computed by exact diagonalization [19] and careful state tracking [29].

-
- [1] A. Di Paolo, T. E. Baker, A. Foley, D. Sénéchal, and A. Blais, *npj Quantum Information* **7**, 11 (2021).
- [2] G. Viola and G. Catelani, *Physical Review B* **92**, 10.1103/physrevb.92.224511 (2015).
- [3] S. Singh, G. Refael, A. Clerk, and E. Rosenfeld, *Impact of Josephson junction array modes on fluxonium readout* (2024).
- [4] D. Ding, H.-S. Ku, Y. Shi, and H.-H. Zhao, *Physical Review B* **103**, 10.1103/physrevb.103.174501 (2021).
- [5] U. Vool and M. Devoret, *International Journal of Circuit Theory and Applications* **45**, 897 (2017).
- [6] D. G. Ferguson, A. A. Houck, and J. Koch, *Physical Review X* **3**, 10.1103/physrevx.3.011003 (2013).
- [7] U. Schollwöck, *Reviews of Modern Physics* **77**, 259–315 (2005).
- [8] U. Schollwöck, *Annals of Physics* **326**, 96–192 (2011).
- [9] G. Vidal, *Physical Review Letters* **91**, 10.1103/physrevlett.91.147902 (2003).
- [10] J. C. Bridgeman and C. T. Chubb, *Journal of Physics A: Mathematical and Theoretical* **50**, 223001 (2017).
- [11] R. Orús, *Annals of Physics* **349**, 117–158 (2014).
- [12] U. Schollwöck, *Annals of Physics* **326**, 96–192 (2011).
- [13] C. Hubig, I. P. McCulloch, and U. Schollwöck, *Physical Review B* **95**, 10.1103/physrevb.95.035129 (2017).
- [14] J. Koch, T. M. Yu, J. Gambetta, A. A. Houck, D. I. Schuster, J. Majer, A. Blais, M. H. Devoret, S. M. Girvin, and R. J. Schoelkopf, *Physical Review A* **76**, 10.1103/physreva.76.042319 (2007).
- [15] S. R. White, *Physical Review B* **72**, 10.1103/physrevb.72.180403 (2005).
- [16] D. E. Parker, X. Cao, and M. P. Zaletel, *Physical Review B* **102**, 10.1103/physrevb.102.035147 (2020).
- [17] E. Rui, Master’s thesis, University of Milan (2023) https://minerva.unimi.it/permalink/39UMI_INST/16hmm17/alma991017855100706031 .
- [18] S. E. Nigg, H. Paik, B. Vlastakis, G. Kirchmair, S. Shankar, L. Frunzio, M. H. Devoret, R. J. Schoelkopf, and S. M. Girvin, *Physical Review Letters* **108**, 10.1103/physrevlett.108.240502 (2012).
- [19] Z. K. Mineev, Z. Leghtas, S. O. Mundhada, L. Christakis, I. M. Pop, and M. H. Devoret, *Energy-participation quantization of Josephson circuits* (2020), [arXiv:2010.00620](https://arxiv.org/abs/2010.00620).
- [20] A. Petrescu, C. Le Calonnec, C. Leroux, A. Di Paolo, P. Mundada, S. Sussman, A. Vrajitoarea, A. A. Houck, and A. Blais, *Physical Review Applied* **19**, 10.1103/physrevapplied.19.044003 (2023).
- [21] J. Williamson, *American Journal of Mathematics* **58**, 141 (1936).
- [22] J. Colpa, *Physica A: Statistical Mechanics and its Applications* **93**, 327–353 (1978).
- [23] M. G. Genoni, L. Lami, and A. Serafini, *Contemporary Physics* **57**, 331–349 (2016).
- [24] A. Serafini, *Quantum Continuous Variables* (CRC Press, 2017).
- [25] G. Citteroni, M. Polini, M. Dapolito, D. N. Basov, and G. Mazza, *Ultrafast dynamics of quantum matter driven by time-energy entangled photons* (2025).
- [26] T. Weißl, B. Küng, E. Dumur, A. K. Feofanov, I. Matei, C. Naud, O. Buisson, F. W. J. Hekking, and W. Guichard, *Physical Review B* **92**, 10.1103/physrevb.92.104508 (2015).
- [27] G. Zhu, D. G. Ferguson, V. E. Manucharyan, and J. Koch, *Physical Review B* **87**, 10.1103/physrevb.87.024510 (2013).
- [28] F. Yilmaz, S. Singh, M. F. S. Zwanenburg, J. Hu, T. V. Stefanski, and C. K. Andersen, *Energy participation ratio analysis for very anharmonic superconducting circuits* (2024).
- [29] J. Cohen, A. Petrescu, R. Shillito, and A. Blais, *PRX Quantum* **4**, 10.1103/prxquantum.4.020312 (2023).